BMC Veterinary Research

RESEARCH

Open Access

Isolation and characterization of goose astrovirus genotype 1 causing enteritis in goslings from Sichuan Province, China

Guo Chen[1,2], Lingdan Yin[1,2] and Huanrong Zhang[1,2*]

Abstract

Since 2017, goose astrovirus (GoAstV) has been widely prevalent in various provinces of China, causing economic losses in the goose industry, with outbreak mortality rates ranging from 10 to 60%. Notably, a goose farm in Sichuan Province has faced an outbreak of infectious disease in 1–3 weeks old goslings, with a mortality rate of approximately 30%. Viral metagenomic analysis of fecal samples identified Goose astrovirus genotype 1 (GoAstV-1), and PCR analysis confirmed the presence of GoAstV-1. Furthermore, we successfully isolated a GoAstV-C1 strain using goose embryos named AAstV/Goose/CHN/2023/C1 (GenBank No. PP108251), and its viral titer was calculated as 10^4.834 ELD_{50}/0.5 mL using the Reed-Muench method. The genome size of GoAstV-C1 was about 7,261 nucleotides through amplifying with Sanger sequencing and assembling with SeqMan software. Phylogenetic analysis revealed that GoAstV-1 strains are classified into three major subtypes: A, B, and C, with the GoAstV-C1 strain identified as a unique variant within subtype B, characterized by distinct genetic divergence features. Experimental inoculation of one-day-old goslings with the virus resulted in a mortality rate of 5 out of 15 (p-value = 0.0421) and a significant reduction in weight gain compared to controls (p-value = 0.005). Pathological examination revealed that GoAstV-C1 infection caused severe damage to the liver, spleen, and kidneys. Interestingly, unlike most GoAstV, which leads to characteristic gout symptoms, our isolates GoAstV-C1 caused obvious intestinal damage characterized by necrosis, inflammatory infiltration, and crypt architectural disruption. We indicated that GoAstV-C1 displays a unique intestinal tropism rather than characteristic gout symptoms and elucidated genomic features and evolutionary relationships of GoAstV strains. These findings help advance our knowledge of the epidemiology and pathogenicity of GoAstV-1, and the predicted structure of capsid protein could serve as a potential target for designing novel antiviral drugs or vaccines against GoAstV-1.

Keywords Viral metagenome, Goose astrovirus genotype 1, Isolation, Phylogenetic analysis, Pathogenicity

*Correspondence:
Huanrong Zhang
22100058@swun.edu.cn
[1]College of Animal and Veterinary Sciences, Southwest Minzu University, Chengdu 610041, PR China
[2]Key Laboratory of Veterinary Medicine of Universities in Sichuan, Chengdu 610041, PR China

Introduction

Astrovirus (AstV) is a non-enveloped, single-stranded, positive-sense RNA virus with an icosahedral structure and approximately 30 nm in the diameter (Yin et al., 2021). The AstV's genome, ranging from 6.4 to 7.9 kb, consists of three open reading frames (ORFs): ORF1a, ORF1b, and ORF2, as well as a 5′-UTR, a 3′-UTR, and a poly(A) tail [15]. ORF1a and ORF1b encode non-structural proteins involved in viral replication and packaging [8], while ORF2 encodes the capsid protein, including a conserved N-terminal domain (VP34) and a variable C-terminal domain (VP27) which serves as the viral neutralizing antigenic determinant [9].

Astroviruses are classified in the Astroviridae family, which is divided into genera Mamastrovirus (MAstV) and Avastrovirus (AAstV). AAstV genus is further divided into AAstV-1, AAstV-2, and AAstV-3 [10]. Like MAstV infections, AAstV infections can cause enteritis in poultry. For example, chicken astrovirus (CAstV) infection can cause runting-stunting syndrome (RSS) in broilers, and turkey astrovirus (TAstV) infection leads to poultry enteritis and mortality syndrome (PEMS) [16, 22]. Previous reports demonstrated that AAstV infection caused diarrhea, growth retardation, and depression, with histopathological changes showing damage to intestinal villi, crypts, and goblet cells [21].

GoAstV was first identified in 2017, and current research has classified it into two genotypes: GoAstV-1 and GoAstV-2 [39]. GoAstV-1 primarily affects goslings between 1 and 3 weeks of age. To date, GoAstV-1 infections have been reported in several provinces, including Hunan, Anhui, Hebei, Shandong, Jiangsu, Jiangxi, Zhejiang, and Guangdong (Fig. 1). Earlier studies have revealed that GoAstV infection of goose can cause mortality rates ranging from 10 to 60% [37], depending on factors such as infection route, viral dose, and host age. For instance, younger goslings (1–15 days old) often exhibit higher mortality rates than older goslings (25–35 days old) due to underdeveloped immune systems [2]. Additionally, variations in the infection route may influence the severity of the disease [28].

In July 2023, an outbreak of infectious disease characterized by enteritis occurred among goslings at a goose farm in Sichuan. To determine the causative agent responsible for the disease, we conducted an in-depth analysis using viral metagenomic sequencing, a widely used method for detecting novel or unexpected pathogens and assessing viral diversity in clinical samples [13, 24]. Our results reveal that unlike previously reported GoAstV causing the characteristic gout symptom, our GoAstV-C1 strain exhibited a distinct intestinal tropism with severe intestinal necrosis, inflammatory infiltration, and crypt architectural disruption, highlighting the

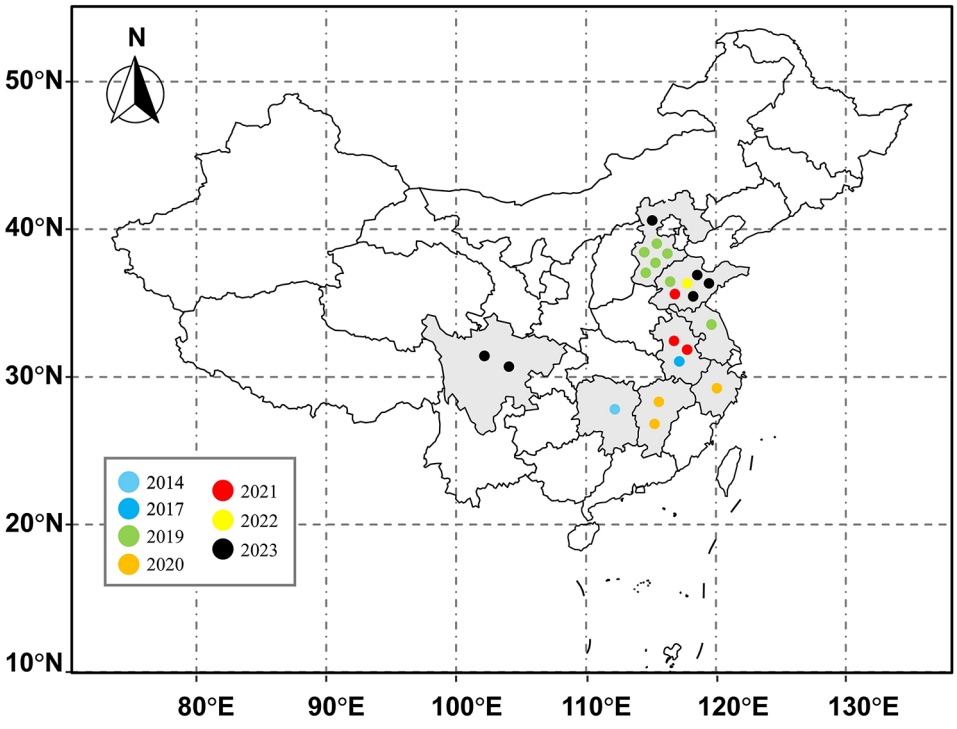

Fig. 1 Spatial and temporal distribution of GoAstV-1 isolates. The figure illustrates the geographical and temporal distribution of GoAstV-1 strains based on location annotations in the metadata of sequence submissions retrieved from the NCBI database. The map highlights the regions and years of reported outbreaks of GoAstV-1 in China

pathogenic diversity among GoAstV strains. This study provides valuable insights into the pathogenesis and epidemiology of GoAstV, with potential implications for future research.

Materials and methods

Viral metagenomic analysis of fecal samples

Disease samples were collected from a goose farm in Sichuan Province, China. Specifically, 30 fecal and tissue samples, including liver, kidney, and intestine, were obtained from the diseased goslings. The fecal samples were diluted in sterile PBS at a ratio of 1:4, vortex-mixed, and then centrifuged at 12,000 rpm at 4 °C for 15 min to collect the supernatant. The supernatant was subsequently filtered through a 0.22-μm filter to remove bacteria. Fifty microliters from each of the 30 treated samples were combined to form a pooled sample of 1.5 mL to increase sample processing efficiency [20]. DNA and RNA were extracted using the FastPure Viral DNA/RNA Mini Kit (Vazyme, Nanjing, China) and were then subjected to library construction and sequencing using the Illumina NovaSeq 6000 platform by Sangon Biotech (Shanghai, China). The sequencing data were analyzed using the viral data analysis platform available at http://www.virome-swun.cn/. Raw reads were first assessed for quality using FastQC and filtered with fastp to remove low-quality reads and adapter sequences. Residual adapters and low-quality bases were trimmed, and the high-quality reads were assembled using SPAdes to reconstruct contigs. The assembled contigs were annotated through BLAST searches against the NCBI nucleotide and protein databases to identify viral sequences.

Pathogen identification in liver tissue samples

Under aseptic conditions, the livers of the diseased goslings were dissected into small pieces and added to sterile PBS at a ratio of 1:4 (W/V). The tissues were thoroughly ground, vortex-mixed, and subjected to three cycles of freeze-thawing to achieve cell lysis and RNA release. The homogenate was then centrifuged at 12,000 rpm for 15 min at 4 °C to collect the supernatant, which was subsequently filtered through a 0.22 μm filter to remove bacteria. The filtrate was stored at -80 °C for future use.

DNA and RNA were extracted from a portion of the filtrate using the FastPure Viral DNA/RNA Mini Kit (Vazyme, Nanjing, China). RNA was reverse transcribed into cDNA using the PrimeScript FAST RT reagent Kit (Takara, Dalian, China). Specific primers reported in the literature were employed to detect common goose viruses in the filtrate, including GoAstV-2, goose parvovirus (GPV), goose hemorrhagic polyomavirus (GHPV), duck Tembusu virus (DTMUV), and goose reovirus (GRV).

Based on the viruses identified in the viral metagenomic analysis of the fecal samples, specific primers were designed using Primer-BLAST (https://www.ncbi.nlm.nih.gov/tools/primer-blast/index.cgi) to detect and valid ate the viruses presented in the viral metagenomic data (Table 1). The PCR reaction system consisted of 10 μL of Takara Premix Taq (2 ×), 1 μL of template, 1 μL each of 10 μM forward and reverse primers, and the final volume

Table 1 Sequences of detection primers

Primer	Primer sequence (5′-3′)	Target	Annealing temperature (℃)	Reference
GoAstV-2	F: AAGCCTCTTTTCTGGCGGATAC	329 bp	62	[34]
	R: GACACAAGCCTATCATCGCCATAG			
GHPV	F: GAGGTTGTTGGAGTGACCACAATG	144 bp	59	[14]
	R: ACAACCCTGCAATTCCAAGGGTTC			
GRV	F: AGGATACAGTGTTCCATCCTG	333 bp	54	[38]
	R: ACTGGATCCAGAGTGCAGAAT			
GPV	F: CTTATTGGAGGGTTCGTTCGT	176 bp	48	[3]
	R: GCATGCGCGTGGTCAACCTAACA			
DTMUV	F: CTGAAGCTTGGAAACTATAATGGCAG	501 bp	58	[40]
	R: GCTGTACGCTGGGGCAATT			
GoAstV-1	F: TGCTGCACAAGTTGGATGGA	828 bp	60	Designed in this study
	R: GGCCCAACTTCTGGTAGCTT			
Goose calicivirus	F: TGCATCTGGGACGAATTTGACAC	269 bp	55	
	R: ACACCTGGGTTCTTCTTCAT			
Goose picornavirus	F: TCGCAAGCCATGAAAAGTGG	395 bp	58.3	
	R: ATGCACATCCCTCTTCCACC			
Goose megrivirus	F: GAGGGTGAGACCACAGTTGG	978 bp	58.1	
	R: TTTTCCATCTGCCCGACTCC			
Rotavirus G	F: AACTCCCGCATCGTATCACC	338 bp	58.5	
	R: TCATCGGCCTCAAACGGAAA			

of 20 μL with double-distilled water (ddH_2O). The reaction conditions were as follows: initial denaturing at 95℃ for 5 min; followed by 35 cycles of denaturing at 94℃ for 30 s, annealing for 30 s according to the temperature in the table, and extension at 72℃ for 1 min; a final extension at 72℃ for 8 min, and preservation at 4℃. The PCR products were then analyzed using 1% agarose gel electrophoresis.

GoAstV-1 isolation from liver samples

The chorioallantoic cavities of three 11-day-old non-immune goose embryos were inoculated with 0.5 mL of filtrate, which tested positive for GoAstV-1 in liver tissues. Embryos that died within 24 h post-inoculation were excluded, as early deaths likely resulted from handling stress or contamination rather than viral infection. Surviving embryos were monitored daily, and dead embryos were collected for analysis. Five days post-inoculation, embryonic bodies and allantoic fluid were harvested and stored at -80℃ for further use. Lesions were assessed based on gross pathological changes, including tissue discoloration, hemorrhages, and structural abnormalities. Blind passages were performed for four generations, each passage involving re-inoculation of the allantoic fluid into new embryos. Viral RNA was confirmed by RT-PCR using primers specific to the GoAstV-1 genome, with positive and negative controls included for validation.

For further analysis, the fourth generation of allantoic fluid was subjected to a ten-fold serial dilution with PBS, resulting in eight dilution groups. Each dilution was inoculated into five 11-day-old goose embryos at a volume of 0.5 mL. The 50% embryo lethal dose (ELD_{50}) was calculated using the Reed-Muench method. The ELD_{50} was calculated using the formula:

$$\mathrm{ELD}_{50} = \text{Lower dose} + \text{Dose interval} \times \frac{50 - \mathrm{P}_{\mathrm{below}}}{\mathrm{P}_{\mathrm{above}} - \mathrm{P}_{\mathrm{below}}}$$

P_{below} and P_{above} are presented as the cumulative positive percentages below and above the 50% threshold. The dose interval is the difference between consecutive doses [6].

To observe the size and morphology of the virus particles, GoAstV-1 positive allantoic fluid was stained with 1% phosphotungstic acid for 2 min at room temperature. The stained samples were then examined using a JEM-1400FLASH transmission electron microscope.

Genomic analysis of GoAstV-1

Based on the GoAstV-1 sequence obtained from the viral metagenome, primers for whole genome amplification were designed using Primer-BLAST (Table 2). The isolated GoAstV-1 cDNA served as a template for amplification using 2 × Phanta Flash Master Mix (Vazyme, Nanjing, China). The PCR reaction system consisted of 25 μL of 2 × Phanta Flash Master Mix, 5 μL of template, 2 μL each of 10 μM forward and reverse primers, and the final volume of 50 μL with ddH_2O. The reaction conditions were as follows: initial denaturing at 98℃ for 30 s; followed by 30 cycles of denaturing at 98℃ for 30 s, annealing at 58℃ for 30 s, and extension at 72℃ for 10 s; a final extension at 72℃ for 1 min, and preservation at 4℃. The PCR products were gel-purified and ligated into the pMD19-T vector (Takara, Dalian, China). The ligated product was transformed into DH5α competent cells (Vazyme, Nanjing, China). Positive clones were identified by sequencing at Sangon Biotech (Shanghai, China).

The whole genome sequence of AAstV was downloaded from the GenBank database. A phylogenetic tree was constructed using the Neighbor-Joining method in MEGA-X software. Genetic distances were calculated

Table 2 Sequences of whole gene amplification primer

Primer	Primer sequence(5′-3′)	Position	Target	Annealing temperature (℃)
1	F: TGCTGCACAAGTTGGATGGA	1–20	1245 bp	61
	R: GGCCCAACTTCTGGTAGCTT	1226–1245		
2	F: AAGCCTCTTTTCTGGCGGATAC	914–933	1475 bp	57.3
	R: GACACAAGCCTATCATCGCCATAG	2369–2388		
3	F: GAGGTTGTTGGAGTGACCACAATG	1966–1988	1331 bp	58
	R: ACAACCCTGCAATTCCAAGGGTTC	3278–3296		
4	F: AGGATACAGTGTTCCATCCTG	3065–3085	1038 bp	58
	R: ACTGGATCCAGAGTGCAGAAT	4083–4102		
5	F: CTTATTGGAGGGTTCGTTCGT	3817–3836	1198 bp	57.5
	R: GCATGCGCGTGGTCAACCTAACA	4992–5014		
6	F: CTGAAGCTTGGAAACTATAATGGCAG	4758–4777	1127 bp	57.6
	R: GCTGTACGCTGGGGCAATT	5865–5884		
7	F: TGCATCTGGGACGAATTTGACAC	5564–5583	1051 bp	59.5
	R: ACACCTGGGTTCTTCTTCAT	6593–6614		
8	F: TCGCAAGCCATGAAAAGTGG	5217–6236	1038 bp	57.6
	R: ATGCACATCCCTCTTCCACC	7234–7254		

using the p-distance method, with the bootstrap value set to 1000. To determine the subtype of GoAstV, we conducted a phylogenetic analysis using the K-means clustering method based on the genetic distance matrix of 22 GoAstV genomes, and the elbow method was employed to ascertain the optimal number of clusters.

ORFs were predicted using ORFfinder (https://www.ncbi.nlm.nih.gov/orffinder/). The proteins encoded by ORF1a, ORF1b, and ORF2 were analyzed using InterPro (http://www.ebi.ac.uk/interpro/search/sequence/). Additionally, the protein encoded by ORF2 and its three-dimensional structure was predicted using SWISS-MODEL, AlphaFold2, and PyMol software.

Experimental infection of goslings

Artificial infection experiments were conducted on goslings to verify the pathogenicity of the GoAstV-1 strain. Thirty 1-day-old goslings were randomly divided into two groups. The goslings in group 1 were inoculated subcutaneously in the neck with 1 mL of the fourth-generation allantoic fluid (10^4.834 ELD_{50}/0.5 mL). The goslings in group 2 were inoculated with 1 mL of sterile PBS and served as the negative control group. The two groups were housed separately in isolated feeding equipment to prevent cross-infection and maintained under identical environmental conditions, including temperature, humidity, and feeding practices, to exclude the possibility of disruption of environmental factors.

At eight specific time points post-infection (1 d, 3 d, 5 d, 7 d, 10 d, 13 d, 16 d, and 21 d), three goslings were randomly selected from each group for weighing. Tissues and organs from any deceased goslings were collected for histopathological examination and pathogen identification.

The Kaplan-Meier method was used to analyze survival data for both groups. The statistical significance of differences in survival probability between the infected and control groups was calculated by a log-rank test [12]. Additionally, chi-squared testing was conducted to assess differences in infection rates and mortality between the groups. These statistical analyses were performed using Python's lifelines and scipy libraries, and p-values < 0.05 were considered statistically significant.

qPCR detection method

The pET-32a(+) standard plasmid containing the ORF1b region of GoAstV-C1, constructed by Sangon Biotech, was used as the template for the subsequent qPCR standard curve. For standard curve construction, the plasmid was verified by sequencing and serially diluted 10-fold to concentrations ranging from 1.0×10^8 to 1.0×10^1 copies/μL. The qPCR reaction system (20 μL total volume) included the following components: 10 μL TB Green Premix Ex Taq II (Takara, Dalian, China), 0.2 μM forward primer (5'-GGTCTGGACAGGCGGATTAGAAG-3'), 0.2 μM reverse primer (5'-CATCATAGCGGGTCCAATCCATTTC-3'), 1 μL of diluted standard plasmid template (final concentration ranging from 1.0×10^8 to 1.0×10^1 copies/μL), and was adjusted the final volume to 20 μL with ddH_2O. The qPCR conditions were pre-denaturation at 95℃ for 30 s, followed by 40 amplification cycles with denaturation at 95℃ for 5 s and annealing at 60℃ for 10 s.

Statistical analyses

All experiments were independently performed at least three times, and data are presented as mean ± standard deviation (SD). Inter-experimental variability was assessed using GraphPad Prism 10.1.2 software (GraphPad Software, Inc.). Differences between samples were analyzed using a t-test, with statistical significance set at a p-value of < 0.05.

Results

Clinical signs and pathological observations

The affected goslings on the farm in Sichuan Province were 1 to 3 weeks old, with a mortality rate of approximately 30%. Clinical findings in the affected goslings included depression, while the dead goslings exhibited opisthotonus and loose faeces around the cloaca. All dead geese were observed for clinical signs, and pathology revealed hepatic hemorrhage and renal pallor; intestines were swollen, and blood vessels were dilated. Additionally, black intestinal contents were presented in some goslings. (Fig. 2), highlighting the severity of the infection and its impact on multiple organs.

Viral metagenomic analysis of fecal samples

To further investigate the viral etiology, fecal samples that met the sequencing requirements were sequenced using the Illumina NovaSeq 6000 platform. After data quality control and the removal of host, fungal, and bacterial genes, a total of 45,378,544 reads were obtained. The sequencing quality was high, with Q30 bases accounting for 95.57% after filtering, and these metrics confirm the data's reliability for genome assembly and analysis. Species classification annotation of the reads revealed that the animal-related viruses in the fecal samples primarily included Goose Picornavirus, Goose Megrivirus, Rotavirus G, Goose Calicivirus, and GoAstV-1 (Fig. 3). Additionally, one nearly full-length GoAstV-1 complete sequence was obtained 8,782 reads were mapped to the GoAstV-1 genome (7,261 bp), achieving an average sequencing depth of approximately 181 × and 100% genome coverage.

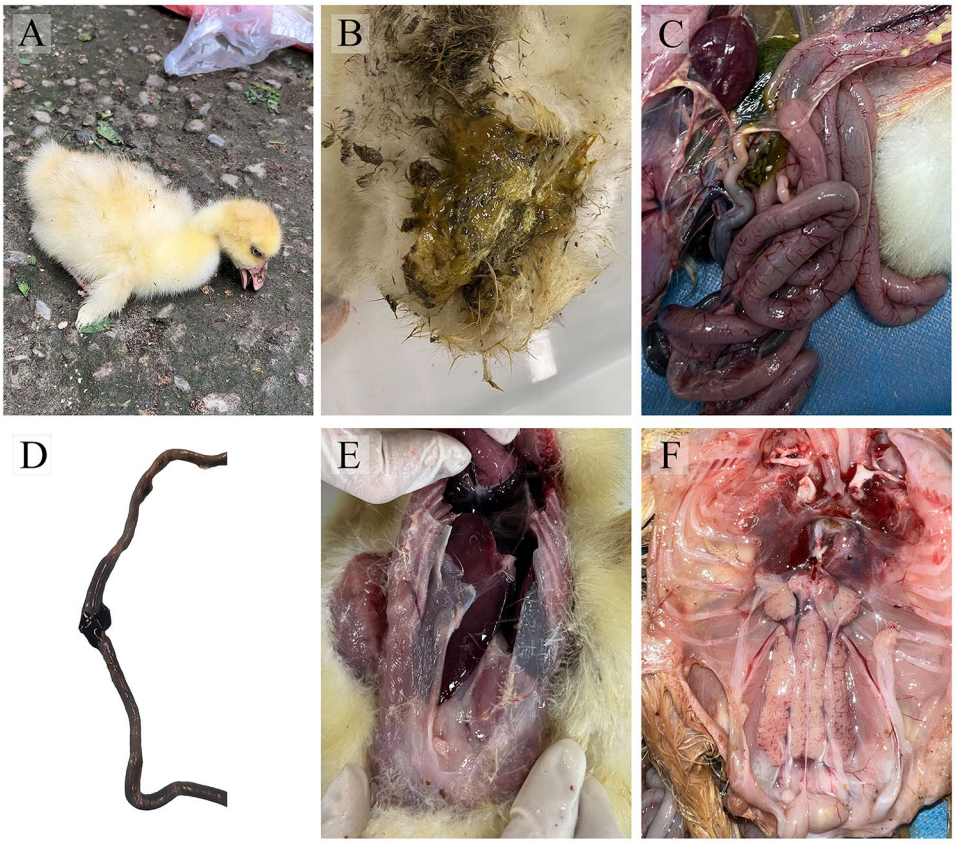

Fig. 2 Clinical and postmortem findings of the affected goslings. (**A**) Affected goslings exhibited signs of depression; (**B**) Loose faeces were observed around the cloaca; (**C**) The intestines of diseased goslings were swollen, and blood vessels were dilated; (**D**) Black intestinal contents were present; (**E**) The liver showed bleeding and swelling; (**F**) The kidneys appeared pale and swollen

Pathogen detection and identification

To further confirm the causative agent responsible for the observed clinical signs and lesions, pathogen detection assays were conducted on tissue samples. A specific PCR test on liver samples revealed that only GoAstV-1 was detected as positive (Supplementary Fig. S1). The positive liver tissue filtrate (0.5 mL) was used to inoculate 10 goose embryos per generation. Two goose embryos from the first generation died, three from the second generation died, six from the third generation died, and all from the fourth generation died. RT-PCR results confirmed that all generations were positive for GoAstV-1. The fourth-generation goose embryos exhibited urate deposition, dead embryo bodies, and liver hemorrhage (Fig. 4). The ELD_{50} of the fourth-generation goose embryo virus was determined to be 10^4.834 ELD_{50}/0.5 mL (Supplementary Table S1). The transmission electron microscopy (TEM) revealed that the viral particles were spherical, approximately 26 nm in diameter, which was consistent with the typical morphology of GoAstV [26]. These results indicate that we successfully isolated the GoAstV-1 strain (Fig. 5).

To verify the concordance of GoAstV-1 in faeces and liver, primers were designed to amplify the complete gene sequence using the GoAstV-1 contig obtained from the viral metagenomic analysis. Eight fragments were successfully amplified (Supplementary Fig. S2), and the full-length genome of GoAstV-1 was obtained through sequencing and splicing. Upon comparison, the viral sequence isolated from the liver was identical to the gene sequence obtained from the viral metagenomic analysis. The GoAstV-1 strain was named AAstV/Goose/CHN/2023/C1 (referred to as GoAstV-C1) and was uploaded to GenBank with the accession number PP108251.

Genome structure and features of GoAstV-C1

The whole genome of the GoAstV-C1 strain was determined to be 7,261 nucleotides (nt) in length. The base composition was as follows: adenine (A) accounted for 32.02%, thymine (T) for 25.75%, cytosine (C) for 18.66%, and guanine (G) for 23.56%. The genome comprised a 5' UTR, three ORFs (ORF1a, ORF1b, and ORF2), and a 3' UTR. The 5' UTR measured 22 nt in length, while the 3' UTR measured 278 nt. ORF1a spanned 3,282 nt (positions 23 to 3,304) and encoded a protein of 1,093 amino acids. This protein contained five transmembrane domains at amino acid positions 217–239, 371–388,

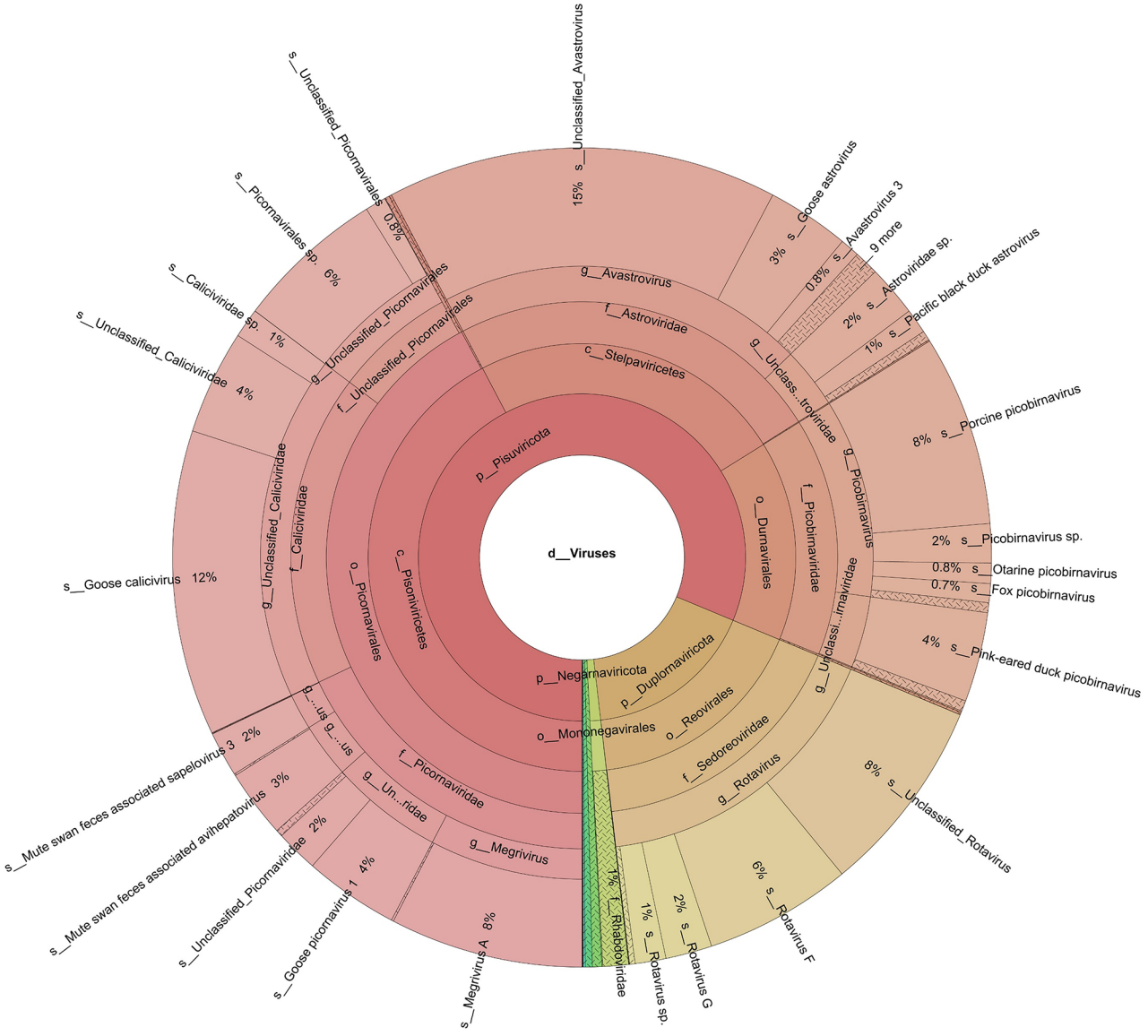

Fig. 3 Krona plot of viral types identified in the library. The Krona plot illustrates the classification and relative abundance of viruses detected in the metagenomic library from fecal samples

401–423, 433–455, and 468–490. It also included three coiled-coil structures at positions 130–161, 166–193, and 748–768. The trypsin-like serine protease domain was located at positions 564–718, and the viral genome-linked protein (VPg) domain spanned positions 784–877, with nuclear localization signals (NLS) at positions 785–799. ORF1a and ORF1b overlapped by 16 nt and contained a seven-base sliding sequence (AAAAAAC). ORF1b was 1,551 nt in length (positions 3,289 to 4,839) and encoded a protein of 516 amino acids. The RNA-dependent RNA polymerase (RdRp) domain was located at positions 260–393. ORF2 was 2,151 nt in length (positions 4,833 to 6,983) and encoded a coat protein of 716 amino acids. Comparative analysis of the amino acid sequences encoded by the ORF2 gene from 22 GoAstV-1 strains revealed that the N-terminus of the ORF2 protein was relatively conserved, whereas the C-terminus was highly variable (Supplementary Fig. S3). The tertiary structure model of the major proteins encoded by ORF2 was predicted and is presented in Fig. 6. The green region, spanning residues 87 to 420, was predicted to constitute the capsid core, forming a stable β-barrel-like structure. The yellow region, spanning residues 437 to 667, was predicted to constitute the capsid spike, forming protruding structures extending from the core.

Phylogenetic analysis

The nucleotide sequence of GoAstV-C1 was phylogenetically analyzed alongside reference sequences of 36 AAstV strains from the GenBank database (Supplementary Fig.

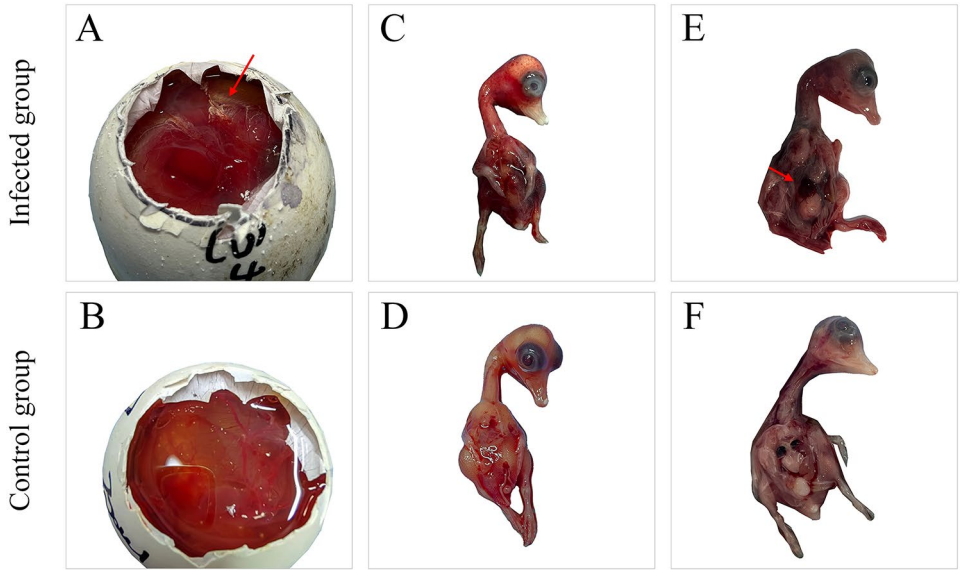

Fig. 4 Lesions observed in goose embryos after inoculation with GoAstV-C1. Uric acid salts were detected in the amniotic fluid (**A**, **B**); Embryonic hemorrhage was observed (**C**, **D**); Hemorrhagic lesions were identified in the liver during postmortem examination (**E**, **F**)

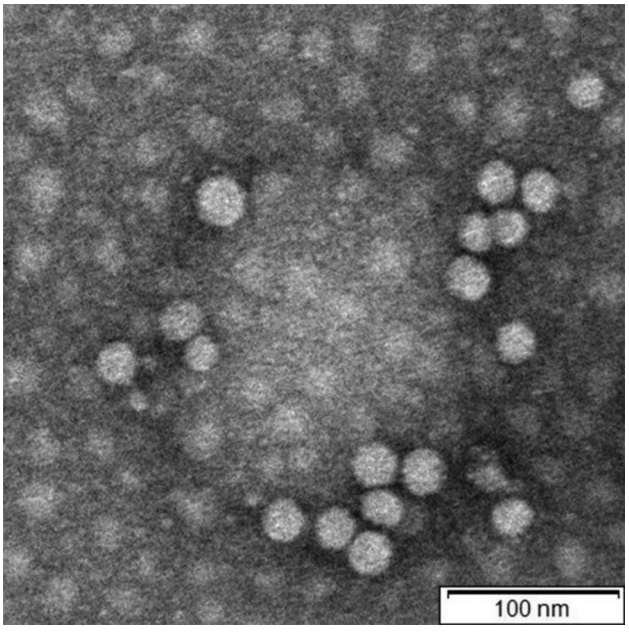

Fig. 5 TEM image of GoAstV-C1 virus particles. Scale bar = 100 nm

S4 and Fig. S5). Based on the complete genome nucleotide sequence and ORF2 amino acid sequence, the phylogenetic trees showed that GoAstV-C1 clustered with the other 21 GoAstV-1 strains. The genetic distance was closest to the A1082, C1330, and C1357 strains isolated in Shandong in 2023 (0.009–0.011), followed by the AH-16 strain isolated in Anhui (0.012). The genetic distance between GoAstV-C1 and other AAstV strains was significantly larger, with the furthest distance observed between GoAstV-C1 and ANV (0.536–0.542). GoAstV-1 could be divided into three main gene subtypes by the

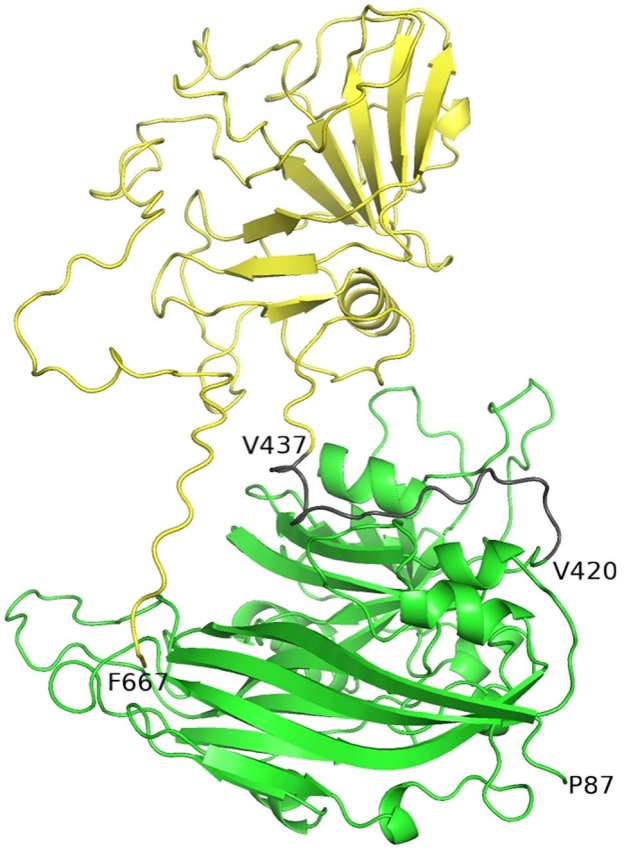

Fig. 6 Predicted tertiary structure of the GoAstV-C1 ORF2 protein. The tertiary structure of the GoAstV-C1 ORF2 protein was predicted using SWISS-MODEL

K-means clustering method: GoAstV-1 A, B, and C. GoAstV-1 A included strains such as FLX, TZ03, and C102. GoAstV-1 C contained the G2332 strain. GoAstV-C1 and the remaining GoAstV-1 strains constituted the GoAstV-1 B subtype. Further identity analysis of the GoAstV-C1 strain with other AAstV strains (Supplementary Table S2) revealed that GoAstV-C1 had the highest identity with the C1357 strain. Compared with the remaining AAstV strains, the genome-wide identity ranged from 44.6% (ANV) to 58.2% (CAstV). The ORF1a amino acid identity ranged from 26.8% (ANV) to 54.8% (DAstV-1). The ORF1b amino acid homology ranged from 52.5% (ANV) to 66.7% (CAstV), and the ORF2 amino acid identity ranged from 28.5% (ANV) to 53.7% (DAstV-2).

Experimental validation of pathogenicity

To validate the pathogenicity of the identified strain and its association with the observed clinical signs, we performed the experimental infections in goslings. Following subcutaneous inoculation with the GoAstV-C1 strain, signs of depression were observed on the third-day post-infection, and five goslings died between days 6 and 13, resulting in a mortality rate of 33.3% (5/15). Kaplan-Meier survival analysis indicated a significant decline in the survival probability of the infected group compared to the control group (log-rank test, p-value = 0.0159). Similarly, the chi-squared test revealed a significant difference in mortality rates between the infected and control groups (p-value = 0.0421) (Fig. 7). The control group exhibited a mean growth rate of 227.37 g (SD = 99.21 g), whereas the infection group had a significantly lower mean growth rate of 160.32 g (SD = 51.13 g), with a statistically significant difference (p-value = 0.005). At 21-day post-infection, the average body weight of the infected group was approximately 25% lower than that of the control group, suggesting that GoAstV-C1 infection significantly impaired gosling growth (Fig. 8). Gross pathology of the five deceased goslings revealed consistent lesions, including black discoloration of the duodenal wall with a foul odor, vascular dilation, and dark intestinal contents. Additional findings included hepatic hemorrhage, pale and enlarged kidneys, and swollen spleens. In contrast, goslings in the control group displayed no clinical signs or deaths (Fig. 9). Histopathological examination of the infected goslings revealed extensive necrosis of the intestinal mucosal layer, with substantial inflammatory and necrotic exudates on the surface of the intestinal lumen. The crypt structures were disrupted, reduced in number, and irregular in shape. In the liver, hepatocytes showed punctate or focal necrosis, accompanied by inflammatory cell infiltration, fibrous tissue proliferation, and congestion and dilation of hepatic sinusoids. The spleen exhibited unclear boundaries between white and red pulp,

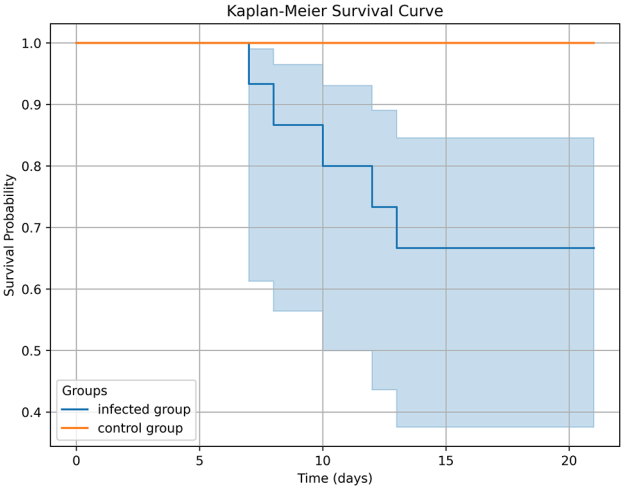

Fig. 7 Kaplan-Meier survival analysis of goslings infected with GoAstV-C1. The Kaplan-Meier survival curve showed a significant reduction in the survival probability of the infected group compared to the control group

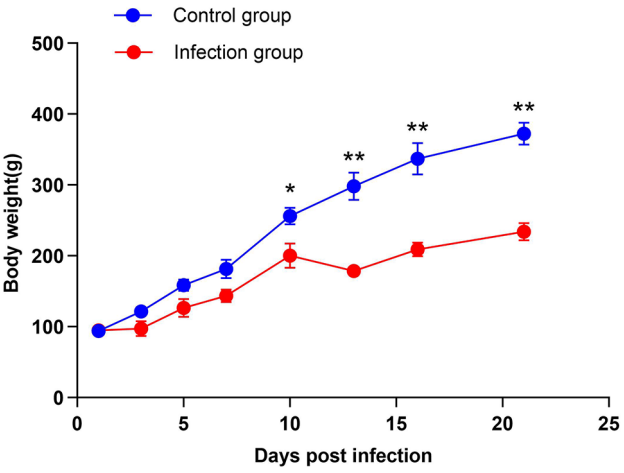

Fig. 8 Weight changes in goslings after infection with GoAstV-C1. p-values were determined by t-test. *$p < 0.05$, **$p < 0.01$

atrophic splenic nodules in the white pulp, a significant reduction in lymphocytes, and degeneration and necrosis of cells in the red pulp. In the kidneys, degeneration and necrosis of renal tubules were observed, with blurred tubular structures (Fig. 10). A qPCR standard curve was constructed using serially diluted plasmid standards (Supplementary Fig. S6). The amplification efficiency was calculated as 107.9%, demonstrating the reliability and stability of the qPCR system. qPCR results demonstrated the presence of GoAstV in various tissues and organs of goslings following subcutaneous inoculation. Among the tested samples, the highest viral load was detected in the intestine, followed by the kidney, bursa of fabricius, liver, spleen, lung, and lymph nodes. The heart and brain observed the lowest viral loads (Fig. 11).

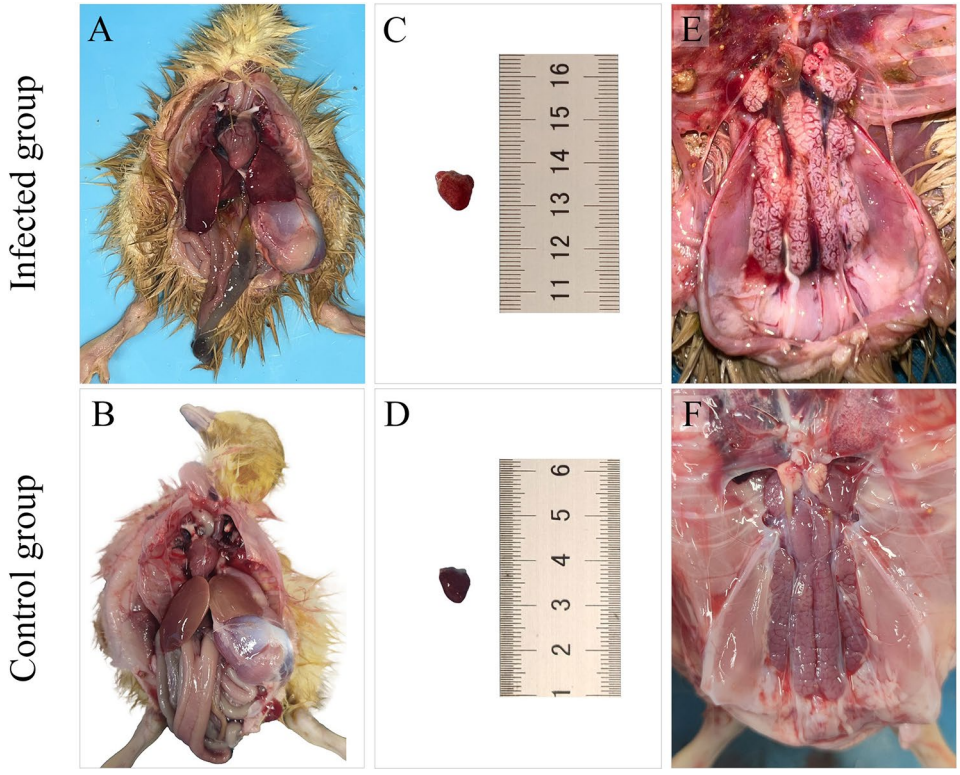

Fig. 9 Postmortem lesions in goslings that died at 8 dpi with GoAstV-C1. The liver exhibited hemorrhaging, and the duodenal wall showed black discoloration with vascular dilation (**A**, **B**); The spleen were enlarged and necrotic with indistinct white and red pulp boundaries (**C**, **D**) ; The kidneys appeared pale and swollen, with visible uric acid deposits (**E**, **F**)

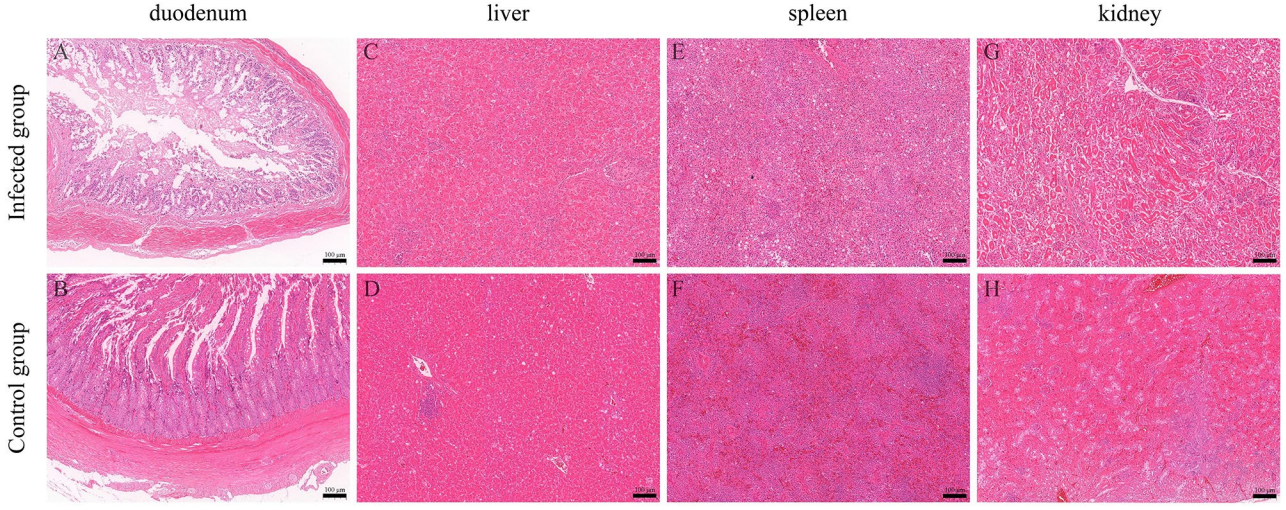

Fig. 10 Histopathological examination of tissues from GoAstV-C1-infected goslings. Necrosis of the intestinal mucosal layer disrupted crypt architecture and inflammatory exudates in the intestinal lumen (**A**, **B**); Hepatocytes exhibited focal or punctate necrosis, accompanied by inflammatory cell infiltration and congestion and dilation of hepatic sinusoids (**C**, **D**); The spleen showed necrosis with atrophic splenic nodules and a significant reduction in lymphocyte count (E, F); Renal tubular degeneration and necrosis in the kidneys (**G**, **H**). Scale bar = 100 μm

Discussion

In July 2023, an infectious disease characterized by enteritis broke out in goslings at a farm in Sichuan, with a mortality rate of approximately 30% among goslings aged 1 to 3 weeks old. Pathogen-specific testing of diseased goslings organ samples detected only GoAstV-1, while other common goose viruses and bacterial infections were ruled out, suggesting a close association between GoAstV-1 and the outbreak. GoAstV-C1 was subsequently isolated from affected goslings through

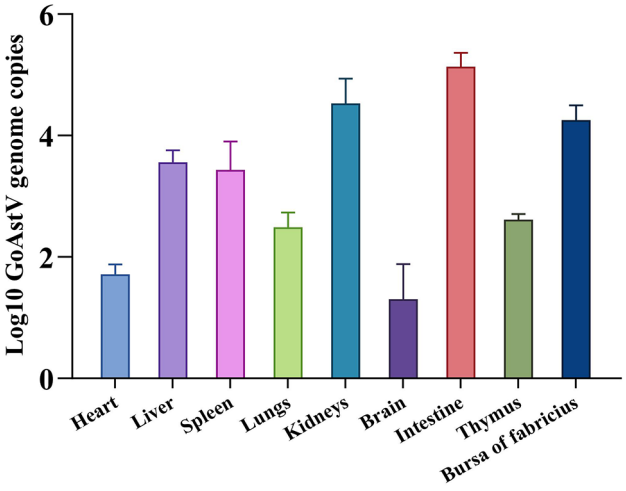

Fig. 11 Viral load of GoAstV-C1 in various tissues of goslings determined by qPCR. The viral load was quantified in different tissues of infected goslings, including the intestine, kidney, bursa of fabricius, liver, spleen, lung, lymph nodes, heart, and brain

the continuous passage in goose embryos. Pathogenicity experiments confirmed its association with the observed outbreak and revealed severe intestinal damage in infected goslings, further establishing the distinctive pathogenic characteristics of GoAstV-C1. These findings offer valuable insights into the pathogenic mechanisms of GoAstV-1 and establish a foundation for studies on its genetic and biological properties.

Presently, the avian embryos or cell lines are usually used to isolate GoAstV strains. For example, GoAstV-2 strains can be isolated using goose embryos [35], chicken embryos [33], duck embryos [4], LMH cells [32], and DF-1 cells [17]. In this study, we selected the goose embryo model for inoculation due to its efficiency in viral propagation and its established application in astrovirus research, allowing for direct observation of embryonic lesions [18]. However, suitable cell lines specifically supporting GoAstV-1 replication are currently lacking, thus greatly limiting the investigations about its replication dynamics, host specificity, and immune evasion mechanisms. Future studies should prioritize the development of advanced cell culture systems capable of supporting GoAstV-1 replication. Such systems would enable more comprehensive research into the biological characteristics and pathogenic mechanisms of GoAstV-1, providing a robust foundation for developing targeted therapeutic and preventive strategies.

GoAstV-C1 possessed the characteristic genomic features of GoAstV, including three ORFs: ORF1a, ORF1b, and ORF2. ORF1a encodes protease domains critical for processing viral polyproteins into functional units necessary for replication. Mutations within these domains may affect replication efficiency and host-virus interactions, as demonstrated in human astroviruses [7]. GoAstV-C1 contained five TM domains based on genetic analysis, whereas strains of GoAstV-2 exhibit only four TM domains, indicating structural differences between the two genotypes. These differences are likely to affect virus translation, replication, and packaging processes, ultimately contributing to variations in pathogenicity [1]. Additionally, GoAstV-C1 harbored a VPg motif, which was essential for initiating the viral replication cycle [25]. The insertions and deletions of this region may promote viral adaptation to cultured cells [30]. ORF1b encoded the RNA-dependent RNA polymerase (RdRp), a vital enzyme for viral genome replication. Its conserved structure may provide the potential target for antiviral therapies, though mutations in RdRp could influence replication fidelity and viral adaptability [27]. The ORF2 region contains a hypervariable segment, which is critical for viral entry into host cells and serves as a primary target for neutralizing antibodies [11]. Variations in this segment may enhance the virus's ability to bind to and infect specific cell types, such as intestinal epithelial cells, through altered receptor interactions or immune evasion mechanisms [19]. These characteristics likely contribute to the unique intestinal tropism of GoAstV-C1. However, whether the specific intestinal pathogenicity of GoAstV-C1 is related to the differences in viral genome structures needs to be further elucidated. In this study, we used SWISS-MODEL to predict the capsid core and capsid spike of GoAstV-C1, laying a foundation for future structural biology validation and functional studies. These computational predictions supplement current knowledge of the GoAstV-1 capsid protein structure. However, SWISS-MODEL has inherent limitations, particularly for astrovirus capsid proteins, as structural database biases and algorithmic assumptions may influence its results [5]. In the future, we will further validate and refine these predictions using advanced techniques such as cryo-electron microscopy and functional assays.

Based on phylogenetic analysis, the currently isolated GoAstV-1 strains were classified into three major subtypes: A, B, and C. Using the K-means clustering method based on the genetic distance matrix of 22 GoAstV genomes and the elbow method to determine the optimal number of clusters [36], we identified three distinct groups that corresponded to the subtypes observed in the phylogenetic tree. Subtype B emerged as the largest cluster, encompassing the majority of genomes and exhibiting a broader geographic distribution compared to the other subtypes. Genetic distance analysis revealed that distances among GoAstV-1 B subtype strains were consistently below 0.1 substitutions per site, indicating gradual evolutionary divergence rather than recent recombination events [23]. Notably, phylogenetic and genetic distance analyses positioned the GoAstV-C1 strain within subtype B but with greater genetic divergence than other

subtype B strains, suggesting it represents a unique variant. This distinct genetic profile may contribute to its novel pathogenic characteristics, including its association with enteritis rather than gout-like symptoms commonly observed in most GoAstV infections. Further analysis revealed that GoAstV-C1 shared an average genetic distance of approximately 0.025 substitutions per site with strains from Shandong, indicating a close genetic relationship and potential cross-regional transmission. These results underscore the importance of continuous surveillance to track the evolutionary dynamics of GoAstV-1 and to identify emerging variants with distinct pathogenic profiles.

Currently, identified pathogenic strains of GoAstV-1 exhibit diverse clinical signs, including urate deposition in organs and joints, mild hemorrhage on the meninges [26], and hepatic and renal necrosis with hemorrhage [29]. In most cases, GoAstV-1 strains are detected in co-infections with GoAstV-2, where gout is the predominant clinical manifestation in goslings [31]. In contrast, our GoAstV-C1 isolate strain infection in goslings caused severe enteritis lesions, which was distinct from the characteristic gout symptoms typically observed in GoAstV infections. Histopathological examinations revealed extensive mucosal necrosis, disrupted crypt structures, and inflammatory necrotic exudates in the intestinal mucosa. In line with the observed severe intestinal lesions, the results of qPCR analysis demonstrated the highest viral load in the intestine, proving that the intestinal damage is attributed to GoAstV-C1. The extensive intestinal damage likely compromised digestive and absorptive functions, leading to the significantly slower growth observed in this experiment. These findings suggest that GoAstV-C1 possesses distinct tissue tropism and distinct pathogenicity compared to other GoAstV strains. However, the underlying mechanisms that determine the pathogenicity differences varying from distinct GoAstV strains are still unclear and need to be investigated in the future.

In summary, we successfully isolated and identified one strain of GoAstV-1, designated as AAstV/Goose/CHN/2023/C1, and demonstrated that enteritis in goslings at the farm is closely associated with GoAstV-C1 infection. Our study underscored that, unlike other GoAstV strains, GoAstV-C1 exhibited an obvious intestinal tropism, which will broaden our knowledge of GoAstV pathogenicity.

Abbreviations

GoAstV	Goose astrovirus
GoAstV-1	Goose astrovirus genotype 1
GoAstV-2	Goose astrovirus genotype 2
TAstV-1	Turkey astrovirus 1
ANV1	Avian nephritis virus 1
ANV2	Avian nephritis virus 2
TAstV-2	Turkey astrovirus 2
DAstV-1	Duck astrovirus 1
CAstV	Chicken astrovirus

Supplementary Information

The online version contains supplementary material available at https://doi.org/10.1186/s12917-025-04482-9.

Supplementary Material 1

Supplementary Material 2

Supplementary Material 3

Acknowledgements

Not applicable.

Author contributions

Huanrong Zhang was responsible for the design of the experiments. Guo Chen was responsible for the execution of the experiments and data analysis, as well as drafting the initial manuscript. Lingdan Yin was responsible for revising the manuscript. All authors read and approved the final manuscript.

Funding

This work was supported by the "Fundamental Research Funds for the Central Universities", Southwest Minzu University (ZYN2024087).

Data availability

Sequence data that support the findings of this study have been uploaded to GenBank with the accession number PP108251.

Declarations

Ethics approval and consent to participate

Animal experiments performed in this study was approved by the Ethical Committee at the College of Animal and Veterinary Sciences, Southwest Minzu University (Approval no. sum-202401005).

Consent for publication

Not applicable.

Competing interests

The authors declare no competing interests.

Received: 25 October 2024 / Accepted: 7 January 2025
Published online: 09 April 2025

References

1 Ali H, Noyvert D, Hankinson J, Lindsey G, Lulla A, Lulla V. The astrovirus N-terminal nonstructural protein anchors replication complexes to the perinuclear ER membranes. PLoS Pathog. 2024;20(7):e1011959.
2 An D, Zhang J, Yang J, Tang Y, Diao Y. Novel goose-origin astrovirus infection in geese: the effect of age at infection. Poult Sci. 2020;99(9):4323–33.
3 Chang PC, Shien JH, Wang MS, Shieh HK. Phylogenetic analysis of parvoviruses isolated in Taiwan from ducks and geese. Avian Pathol. 2000;29(1):45–9.
4 Chen H, Zhang B, Yan M, Diao Y, Tang Y. First report of a novel goose astrovirus outbreak in Cherry Valley ducklings in China. Transbound Emerg Dis. 2020;67(2):1019–24.
5 Chen L, Li Q, Nasif KFA, Xie Y, Deng B, Niu S, Pouriyeh S, Dai Z, Chen J, Xie CY. 2024. AI-Driven Deep Learning Techniques in Protein Structure Prediction. Int J Mol Sci 25(15).
6 Choy MM, Gubler DJ. Isolation and titration of dengue viruses by the mosquito inoculation technique. Methods Mol Biol. 2014;1138:15–25.
7 Cortez V, Meliopoulos VA, Karlsson EA, Hargest V, Johnson C, Schultz-Cherry S. Astrovirus Biology and Pathogenesis. Annu Rev Virol. 2017;4(1):327–48.
8 Cui D, Li S, Yin B, Li C, Zhang L, Li Z, Huang J. Rapid Rescue of Goose Astrovirus Genome via Red/ET Assembly. Food Environ Virol. 2024;16(3):297–306.

9 Dai G, Huang X, Liu Q, Li Y, Zhang L, Han K, Yang J, Liu Y, Xue F, Zhao D. Identification of a linear epitope in the capsid protein of goose astrovirus with monoclonal antibody. Pol J Vet Sci. 2022;25(4):579–87.
10 Donato C, Vijaykrishna D. 2017. The Broad Host Range and genetic diversity of mammalian and avian astroviruses. Viruses 9(5).
11 Espinosa R, Lopez T, Bogdanoff WA, Espinoza MA, Lopez S, DuBois RM, Arias CF. 2019. Isolation of neutralizing monoclonal antibodies to human astrovirus and characterization of Virus variants that escape neutralization. J Virol 93(2).
12 Etikan I. 2017. The Kaplan Meier Estimate in Survival Analysis. Biometrics Biostatistics Int J 5(2).
13 Fitzpatrick AH, Rupnik A, O'Shea H, Crispie F, Keaveney S, Cotter P. High throughput sequencing for the detection and characterization of RNA viruses. Front Microbiol. 2021;12:621719.
14 Guerin JL, Gelfi J, Dubois L, Vuillaume A, Boucraut-Baralon C, Pingret JL. A Novel Polyomavirus (Goose Hemorrhagic Polyomavirus) is the Agent of Hemorrhagic Nephritis Enteritis of Geese. J Virol. 2000;10(74):4523–9.
15 Jin M, Wang X, Ning K, Liu N, Zhang D. Genetic characterization of a new astrovirus in goslings suffering from gout. Arch Virol. 2018;163(10):2865–9.
16 Kang K, Linnemann E, Icard AH, Durairaj V, Mundt E, Sellers HS. Chicken astrovirus as an aetiological agent of runting-stunting syndrome in broiler chickens. J Gen Virol. 2018;99(4):512–24.
17 Li J, Hu W, Liu T, Zhang H, Opriessnig T, Xiao C. Isolation and evolutionary analyses of gout-associated goose astrovirus causing disease in experimentally infected chickens. Poult Sci. 2021;100(2):543–52.
18 Liu C, Sun M, Liao M. 2022. A Review of Emerging Goose Astrovirus Causing Gout. Biomed Res Int 2022:1635373.
19 Martella V, Pinto P, Tummolo F, De Grazia S, Giammanco GM, Medici MC, Ganesh B, L'Homme Y, Farkas T, Jakab F, Banyai K. Analysis of the ORF2 of human astroviruses reveals lineage diversification, recombination and rearrangement and provides the basis for a novel sub-classification system. Arch Virol. 2014;159(12):3185–96.
20 Mortimer J. Intersecting pools and their potential application in testing donated blood for viral genomes. Vox Sang. 1997;73(2):93–6.
21 Raji AA, Omar AR. 2022. An insight into the molecular characteristics and Associated Pathology of Chicken Astroviruses. Viruses 14(4).
22 Shehata AA, Basiouni S, Sting R, Akimkin V, Hoferer M, Hafez HM. Poult Enteritis and Mortality Syndrome in Turkey poults: causes, diagnosis and preventive measures. Anim (Basel). 2021;11(7):2063.
23 Spencer CCA, Deloukas P, Hunt S, Mullikin J, Myers S, Silverman B, Donnelly P, Bentley D, McVean G. The influence of recombination on human genetic diversity. PLoS Genet. 2006;2(9):e148.
24 Sun Y, Qu Y, Yan X, Yan G, Chen J, Wang G, Zhao Z, Liu Y, Tu C, He B. Comprehensive evaluation of RNA and DNA viromic methods based on species richness and abundance analyses using Marmot rectal samples. mSystems. 2022;7(4):e43022.
25 Velazquez-Moctezuma R, Banos-Lara MDR, Acevedo Y, Mendez E. Alternative cell lines to improve the rescue of infectious human astrovirus from a cDNA clone. J Virol Methods. 2012;179(2):295–302.
26 Wang AP, Zhang S, Xie J, Gu LL, Wu S, Wu Z, Liu L, Feng Q, Dong HY, Zhu SY. Isolation and characterization of a goose astrovirus 1 strain causing fatal gout in goslings, China. Poult Sci. 2021;100(11):101432.
27. Wang H, Zhu Y, Ye W, Hua J, Chen L, Ni Z, Yun T, Bao E, Zhang C. Genomic and epidemiological characteristics provide insights into the phylogeographic spread of goose astrovirus in China. Transbound Emerg Dis. 2022;69(5):e1865–76.
28. Wang A, Xie J, Wu Z, Liu L, Wu S, Feng Q, Dong H, Zhu S. Pathogenicity of a goose astrovirus 2 strain causing fatal gout in goslings. Microb Pathog. 2023;184:106341.
29 Wei F, He D, Wu B, Diao Y, Tang Y. 2024. Isolation, identification, and pathogenicity of a Goose Astrovirus Genotype 1 strain in goslings in China. Viruses 16(4).
30 Willcocks MM, Ashton N, Kurtz JB, Cubitt WD, Carter MJ. Cell culture adaptation of astrovirus involves a deletion. J Virol. 1994;68(9):6057–8.
31 Xiang Y, Chen M, Sun M, Dong J, Zhang J, Huang Y, Zhai Q, Liao M, Li L. Isolation, identification, and epidemiological characteristics of goose astrovirus causing acute gout in Guangdong province, China. Poult Sci. 2024;103(10):104143.
32 Xu L, Wu Z, He Y, Jiang B, Cheng Y, Wang M, Jia R, Zhu D, Liu M, Zhao X, Yang Q, Wu Y, Zhang S, Huang J, Ou X, Sun D, Cheng A, Chen S. Molecular characterization of a virulent goose astrovirus genotype-2 with high mortality in vitro and in vivo. Poult Sci. 2024;103(5):103585.
33 Yang J, Tian J, Tang Y, Diao Y. Isolation and genomic characterization of gosling gout caused by a novel goose astrovirus. Transbound Emerg Dis. 2018;65(6):1689–96.
34 Yang L, Yingzi L, Gejin L, Qifeng C, Wang J, Shu X, Zhou T, Gao S. 2021. Establishment of RT-PCR for detection of goose astrovirus. Mod J Anim Husb Veterinary Med(4):1–4.
35 Yuan X, Meng K, Zhang Y, Yu Z, Ai W, Wang Y. 2019. Genome analysis of newly emerging goose-origin nephrotic astrovirus in China reveals it belongs to a novel genetically distinct astrovirus. Infection, Genetics and Evolution: Journal of Molecular Epidemiology and Evolutionary Genetics in Infectious Diseases 67:1–6.
36. Zhang Q, Jun S, Leuze M, Ussery D, Nookaew I. Viral phylogenomics using an alignment-free method: A Three-Step Approach to determine optimal length of k-mer. Sci Rep. 2017;7:40712.
37. Zhang F, Li H, Wei Q, Xie Q, Zeng Y, Wu C, Yang Q, Tan J, Tan M, Kang Z. Isolation and phylogenetic analysis of goose astrovirus type 1 from goslings with gout in Jiangxi Province, China. Poult Sci. 2022;101(7):101800.
38 Zhang X, Chen G, Liu R, Guo J, Mei K, Qin L, Li Z, Yuan S, Huang S, Wen F. Identification, pathological, and genomic characterization of novel goose reovirus associated with liver necrosis in geese, China. Poult Sci. 2024;103(2):103269.
39 Zhu Q, Sun D. Goose Astrovirus in China: a Comprehensive Review. Viruses. 2022;14(8):1759.
40 Zhu S, Tang Y, Diao Y. Development and biochemical characteristics of a monoclonal antibody against prM protein of Tembusu virus. Poult Sci. 2023;102(12):103065.

Publisher's note